IEEE Access
Multidisciplinary | Rapid Review | Open Access Journal

Received 12 October 2022, accepted 18 October 2022, date of publication 25 October 2022, date of current version 7 November 2022.

Digital Object Identifier 10.1109/ACCESS.2022.3216858

RESEARCH ARTICLE

A Novel Miniaturized mmWave Antenna Sensor for Breast Tumor Detection and 5G Communication

CHINMOY DAS[1], MOSTAFA ZAMAN CHOWDHURY[1], (Senior Member, IEEE), AND YEONG MIN JANG[2], (Member, IEEE)

[1]Department of Electrical and Electronic Engineering, Khulna University of Engineering & Technology, Khulna 9203, Bangladesh
[2]Department of Electronics Engineering, Kookmin University, Seoul 02707, South Korea

Corresponding authors: Mostafa Zaman Chowdhury (mzceee@ieee.org) and Yeong Min Jang (yjang@kookmin.ac.kr)

This work was supported by Institute of Information & Communications Technology Planning & Evaluation (IITP) grant funded by the Korea government (MSIT) (No.2022-0-00590, Industrial small cell system supporting 5G multi-band), and in part by the MSIT (Ministry of Science and ICT), Korea, under the ITRC (Information Technology Research Center) support program (IITP-2022-2018-0-01396) supervised by the IITP (Institute for Information & Communications Technology Planning & Evaluation).

ABSTRACT Breast cancer is one of the deadliest forms of disease that affects women worldwide. X-ray mammography, magnetic resonance imaging, and ultrasound are all helpful methods of medical imaging, but they have their own limitations due to low tissue contrast and side effects. Millimeter wave (mmWave) imaging has been offered as a viable alternative to the conventional screening methods due to their drawbacks. Without exposing the patient to ionizing radiations, malignant lesions can be detected by using the dielectric discontinuities in the tissues. The purpose of this work is to develop a simple, low-cost miniaturized mmWave imaging antenna sensor that can be used to detection of breast tumors or cancers in women by monitoring the changes in the antenna's S_{11} parameter. The dimension of the proposed rectangular mmWave antenna is 5 mm $\times$ 5 mm $\times$ 0.578 mm. The proposed antenna sensor has an operating frequency band range of 32.626 GHz to 33.96 GHz with a peak gain of 6.65 dB and an efficiency of 91.46% in terms of radiation which makes it a suitable system for fifth generation (5G) communication. As well as the antenna sensor can detect very tiny malignant that size $\geq$1 mm inside the breast fantom.

INDEX TERMS 5G, breast-tumor, mmWave-imaging, radiation efficiency, SAR, S-parameter.

I. INTRODUCTION

The millimeter wave (mmWave) frequency band has gained popularity for imaging technology in recent years due to their ability to pass through poor weather and other blocking materials including clothing, polymers, and even human muscle. Within the electromagnetic spectrum, mmWave band is defined in the 30 GHz to 300 GHz range with corresponding wavelengths between 10 mm to 1 mm. It is safe for humans to be exposed to radiation at these frequencies since it is non-ionizing. Applications of this technique include the identification of hidden weapons, explosives, and cancer cells in the human body. mmWave imaging is a very promising technique to detect brain tumor, brain cancer, breast tumor, and breast cancer in the human body as well [1].

The most commonly diagnosed and deadliest kind of cancer is the lung cancer, (which accounts for 11.6% of all cases) and 18.4% of the total cancer deaths for both males and females [1]. After lung cancer, female breast cancer is the most fatal cancer all around the world. According to recent studies, approximately one in eight women develop breast cancer during their lifetime. Female breast cancer is one of the leading causes of cancer death worldwide (6.6% of the total cancer deaths) [1]. There are 154 nations in the world where breast cancer is the top cause of cancer death among women. As of 2018, it is estimated that almost half of all cases of breast cancer in the globe, and more than half of all deaths from breast cancer, happened in only Asia [1]. In the last year, 685,000 women were dead and approximately 3 million

The associate editor coordinating the review of this manuscript and approving it for publication was Mehdi Sookhak.

women will be diagnosed with breast cancer worldwide in 2022. In over 100 nations, it is the leading cause of cancer-related death and is by far the most often diagnosed form of the disease [2].

It has been confirmed that to save lives, proper treatment methods and health screenings effectively promote the early detection of tumor cells [3]. Regular screenings are essential in the direction of early diagnosis of breast tumors. Ultrasound, magnetic resonance imaging (MRI), and X-ray mammography have all been used traditionally for breast imaging, but only the latter is employed for screening in some countries. This is due to the fact that ultrasonic imaging is strongly dependent on the ability of the physician who performs it and it fails when there is bone and air present. It is also not suitable for breasts with high-fat content, while the major drawback of MRI is its huge cost [4], [5]. Contrary to popular belief, X-ray mammography exposes women to ionizing radiation, which carries its own set of dangers when performed regularly and this method has a fair amount of false positive or false negative readings because of the lack of contrast between healthy tissue and tumor [6]. Even though there are health risks associated with ionizing radiation exposure, many women find mammography to be uncomfortable and painful as well [7]. Ionized radiation makes these procedures unsuitable, in particular, for younger women.

As a result, new microwave imaging (MWI) methods are being developed. Because of its low cost, low profile, mobility, and non-ionizing effects, MWI is a cutting-edge medical diagnostic tool that has drawn a lot of attention in the fields like breast tumor detection, brain tumor detection, early-stage heart failure diagnosis, and health monitoring. In this type of process, microwaves are transmitted through the human body via a transmitting antenna, which also works as a transceiver. After then, the antenna is used to gather data. MWI antenna sensors can discriminate between microwave signals scattered from different tissues in the human body. For further processing, the antenna sensors receive the radiated and scattered energy.

The existing MWI techniques for breast cancer detection operate in the microwave frequency range of 10 to 15 GHz. Even a 15 GHz to 20 GHz range has been achieved by some researchers but it is not enough to detect small malignant like 5 mm or smaller tumor size [8] and this is one of the drawbacks of the previous works. On the other hand, the data on the relative permittivity of human skin tissues has only been available for frequencies under 20 GHz for more than a decade [9]. Afterwards in 2017, with the help of spectroscopy [10], the dielectric characteristics of skin tissues at mmWave are determined. In mmWave imaging, the image resolution for the smaller size tumors ($<$5 mm) can be improved by at least three times by using the $>$30 GHz and higher band [11]. This bandwidth is also emerging for fifth-generation (5G) communication due to the projected benefits of increased multi-gigabit peak data speeds, ultra-low latency, improved reliability, massive network capacity, and a more consistent user experience.

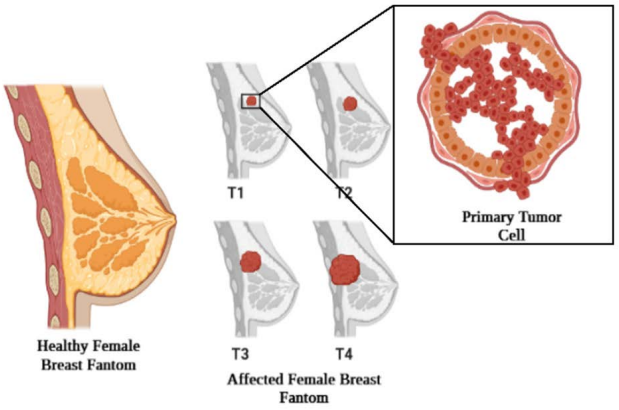

FIGURE 1. Healthy female breast fantom and tumor cell affected female breast fantom anatomy.

This research proposed a mmWave antenna sensor that is very promising to diagnose the early-stage tumor and detect the very smaller size of malignant. Initial experiments demonstrate that an operating frequency greater than 30 GHz can detect a 1 mm size tumor in breast fantom. This proposed antenna system with that high-frequency range can also be used in 5G and beyond high-speed communication by enhancing the gain and the efficiency properly [12]. Smaller, faster, and with greater bandwidth antenna technologies are needed for the 5G communication infrastructure. Single-element microstrip mmWave antennas can be a great candidate for 5G communication systems as well [13] and [14]. The center frequency of the proposed system is set at 35 GHz. A wide bandwidth, ranging from 30 GHz to 40 GHz is also being considered to improve the resolution of the mmWave images. The main advantage of this proposed antenna sensor is that it has also the ability to detect very tiny tumor cells ($\geq$1 mm i.e., stage-1) in breast fantom with a tolerable Specific Absorption Rate (SAR).

The remaining paper is organized as follows. In Section II, the methodology of mmWave imaging is explained. Then the design procedure of breast fantom is presented in Section III. In Section IV, the process of designing the antenna sensor is described briefly. Afterwards in Section V, the results are analyzed in detail. Finally, the study is wrapped up in Section VI by outlining the potential use of the work in the context of mmWave imaging.

II. METHODOLOGY OF mmWave IMAGING

When a normal breast cell undergoes genetic abnormalities, known as mutations, this causes tumor and later cancer development. These alterations occur in genes that affect cell development. Before a cancer cell emerges, these alterations can take years or even decades to take place. The tumor cells multiply and divide exponentially so that one cell becomes two, two cells become four and so on. That is why tumors grow more quickly as they get bigger within a short period of time [15]. Fig. 1 shows a healthy female breast fantom and a breast fantom anatomy affected by tumor cells.

The tumor's volume growth to double is an effective technique to estimate the rate at which breast cancer spreads. The time it takes for a tumor to double in size is called ''doubling time''. On average, breast cancers in younger women grow faster than in older women. Even they also develop a more aggressive tumor cells. A breast cancer's ability to spread is determined by its 4 stage (from stage T1 to stage T4), which ranges from early-stage to advanced and all stages are considered invasive. It is very important to diagnose at an early stage (I&II) because it indicates the cancer has the potential to spread beyond the breasts [16].

At early-stage (T1, T2) breast cancer is considered completely curable. Early detection of breast cancer increases the chances of successful treatment. Regular mammography screening and self-examination are essential to prevent breast cancer. However, most of the time mammography and self-examination cannot determine the early-stage tumor (T1). Exactly how long it takes for a cancerous tumor to develop from a single cancer cell is unpredictable. To some extent, this is because tumor growth is assumed to have a fixed rate of doubling time. It would take 20 years for a cancer cell to develop from a tumor cell that has a doubling time of 200 days and 10 years with a doubling time of 100 days. In contrast, it would only take two years for breast cancer with a 20-day doubling time to develop [17], [18].

Because of the tumor's and healthy tissue's dielectric properties variation, the mmWave imaging method can distinguish the tumor from the surrounding healthy tissue more precisely. The mmWave frequencies are reflected differently by tumors and healthy tissues, and this principle is used to develop a viable system for detecting malignant or tumor cells. A transmitting antenna (Antenna-1) is used to send mmWave pulses to the suspected area of human tissue. In order to detect tumors, backscattering signals are picked up by the reception antenna (Antenna-2) and evaluated the signals using a proper processing system. To achieve high resolution and accurate images requires a compact antenna that radiates signals over a higher frequency range while maintaining the waveform across a large angular range in the millimeter bandwidth.

The two identical antenna acts as a sensor system in a mmWave imaging system. As it can be characterized the breast-tissue properties in terms of permittivity and tangent loss which show the homogeneous properties of the tissues. These properties interact with the transmitted electromagnetic signals. Due to the tumor cell that is exhibited inside the breast fantom the homogeneity of the breast tissues is hampered. As a result, the electromagnetic signals are varied. The variation of the electrical material property of the breast tissue is observed in the result of the transmission coefficient which is also called the scattering matrix or reflection coefficients.

Simply, the mmWave signals from Antenna-1 to Antenna-2 are impacted due to the presence of the tumor cell inside the breast fantom. As the operating bandwidth of the proposed antenna is between 30-40 GHz, it is a great choice for a 5G antenna in a 5G communication system. Since this is initially a 2-port network, the entire system is defined by using the scattering matrix or S-matrix. Because of the two ports, there are 4 elements (S_{11}, S_{22}, S_{21}, S_{12}) in S-matrix which are defined in Fig. 2.

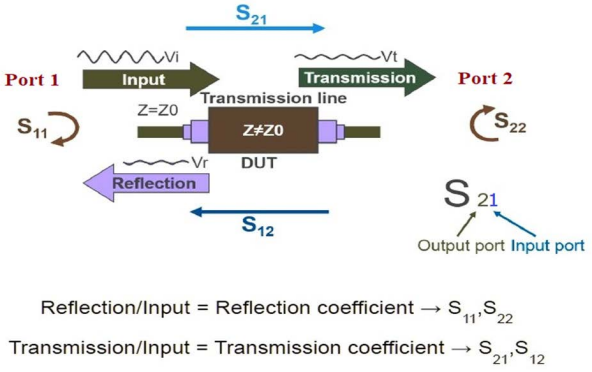

FIGURE 2. Scattering matrix parameters (S_{11}, S_{22}, S_{21}, S_{12}).

III. DESIGN PROCEDURE OF THE BREAST FANTOM

During the design of the breast phantom anatomy, three layers are taken into consideration: skin, adipose tissue, and glandular tissue as shown in Fig. 3. A tumor cell is placed inside the glandular tissue as shown in Fig. 4. The breast phantom is constructed and measured by the methods given in below. The dielectric properties of numerous human body tissues are considered by permittivity and tangent loss. Different tissues have different permittivity and tangent loss values at different frequencies.

The electrical properties of human body tissues are varied with the frequency which is reported in the Cole-Cole dispersion model expression [9] can be expressed as (1).

$$\varepsilon_r(\omega) = \varepsilon_r'(\omega) - j\varepsilon_r''(\omega) = \varepsilon_{ro}(\omega) + \frac{\Delta\varepsilon_r}{1 + (j\omega\tau)^{1-\alpha}} + \frac{\sigma_s}{j\omega\varepsilon_0} \quad (1)$$

where f is the operation frequency, angular velocity $\omega = 2\pi f, j = -1^{1/2}, \tau$ is the relaxation time, $\Delta\varepsilon_r$ is the magnitude of the dielectric dispersion, ε_{ro} is the relative permittivity at optical frequencies, ε_0 is the permittivity of the free space, α denotes broadening of the dispersion, and σ_s is the ionic conductivity of tissues.

A simplified model of a female breast fantom is used to represent the structure of the breast which is shown in Fig. 3. The radius of the breast fantom is considered 12 mm. The thickness of the skin layer is considered 2 mm. The breast fat layer is placed under the breast skin with a thickness of 2 mm and the third layer is the thickest layer inside the fat layer is the fibro-glandular layer (muscle tissue). To represent the breast tumor tissue, a spherical shape is created and positioned within the fibro-glandular layer. For the simulations, a diameter of 1 mm to 3 mm is chosen for tumor. Permittivity and conductivity are the two primary dielectric parameters that are taken into account when studying

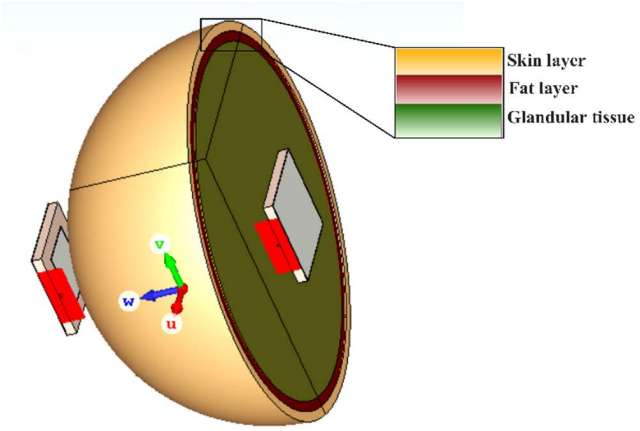

FIGURE 3. Breast fantom anatomy model in CST environment.

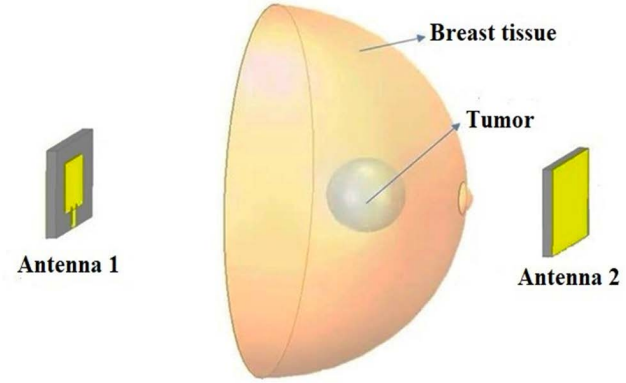

FIGURE 4. Simulation setup model of the system with breast fantom and tumor.

TABLE 1. Breast tissue properties at 33 GHz were considered for the breast model.

Tissues	ε_r	tan δ	Reference
Skin (wet)	17.7	0.93	[19]
Adipose tissue	3.4	0.16	[3]
Fibro glandular	16	0.94	[8]
Tumor	18	1.05	[8]

microwave propagation in live tissue. Electrical fields and magnetic fields can be measured in various structures by comparing the permittivity and conductivity, which vary from material to material. Electromagnetic field values are varied for structures with different biological qualities because they have different permittivity and conductivity values. This factor is crucial in identifying malignant tissue. The fundamental breast structure's permittivity and conductivity values are listed in Table 1.

IV. DESIGN METHODOLOGY OF THE PROPOSED ANTENNA

The maximal pattern in a microstrip patch should be perpendicular to the patch's surface. Selecting the proper excitation mode below the patch accomplishes this job.

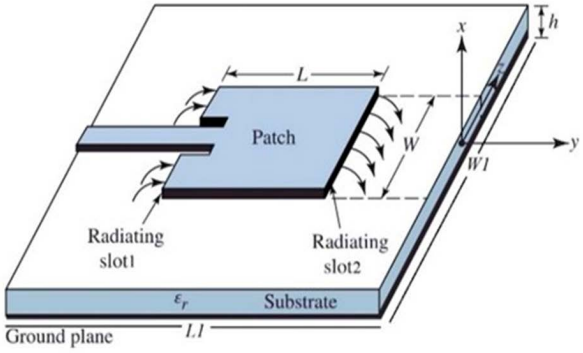

FIGURE 5. The geometric diagram of the proposed mmWave antenna.

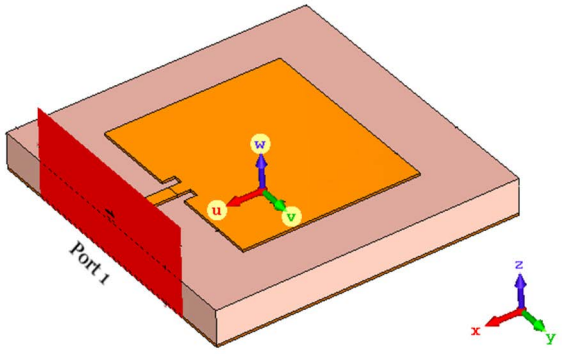

FIGURE 6. The designed model of the antenna sensor in CST (side-view).

Mode selection is another means by which end-fire radiation can be produced. The element's length L for a rectangular patch is typically $\lambda_0/3 \langle L \langle \lambda_0/2$, where λ_0 is the free-space wavelength. The dielectric material (substrate) separates the ground plane and strip (patch) which is depicted in Fig. 5. The dimension (L1×W1) of the antenna is 5 mm × 5 mm. The antenna is fabricated on a dielectric substrate called Roger RT 5880 (lossy) with a thickness of 0.50 mm (relative permittivity, $\varepsilon_r = 2.2$). The CST-designed model is shown in Fig. 6 as well.

The bottom ground plane metal layer thickness is 0.035 mm. The radiating patch dimension (L×W) is 2.75 mm × 3.10 mm with a thickness of 0.035 mm as calculated by (2) and (3), respectively.

$$L = \frac{1}{2f_r\sqrt{\epsilon_{reff}}\sqrt{\mu_0\,\epsilon_0}} - 2\Delta L \tag{2}$$

$$W = \frac{1}{2f_r\sqrt{\mu_0\,\epsilon_0}}\sqrt{\frac{2}{\epsilon_r+1}} = \frac{v_0}{2f_r}\sqrt{\frac{2}{\epsilon_r+1}} \tag{3}$$

where f_r is the resonant frequency, ε_{reff} is the effective dielectric constant, ΔL is the extended length of patch due to the fringing field effect, μ_0 and ε_0 are the permeability and permittivity of free space, respectively, and v_0 is the free-space velocity of light.

The resonant frequency of the microstrip antenna is a function of the antenna's length for the dominant TM_{010} mode.

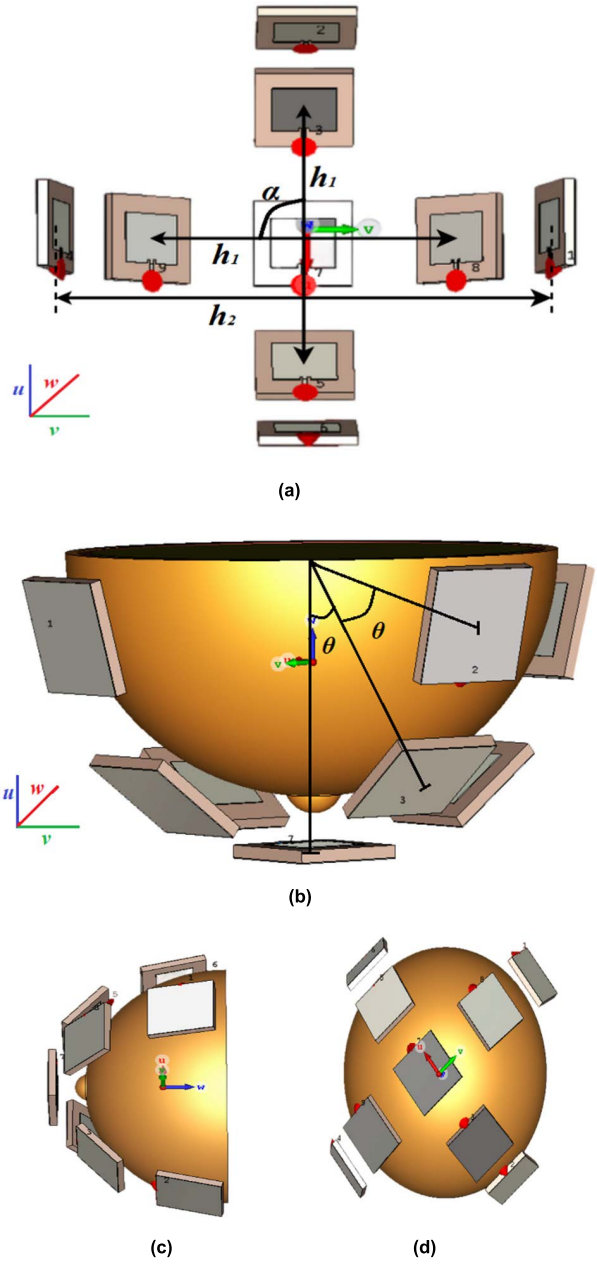

FIGURE 7. Proposed array setup for the breast imaging: (a) 2 cross-sectional array antenna model, (b) angular distance of array elements with breast fantom, (c) side view, and (d) back view.

It can be expressed as,

$$(f_r)_{010} = \frac{1}{2L\sqrt{\epsilon_r}\sqrt{\mu_0\,\epsilon_0}} = \frac{v_0}{2L\sqrt{\epsilon_r}} \tag{4}$$

The microstrip feed line is similarly a conducting strip, however, its width is often much narrower than that of the patch. The microstrip-feed length of 0.975 mm and the width of the feedline are taken to 0.2 mm in order to match the 50 Ω coaxial line. Matching with the transmission line is typically done by adjusting the feed line width and slot length. Fields at the patch's boundaries experience fringing because the patch's dimensions are finite along its length and width. The microstrip antenna has two radiating slots along its length, as seen in Fig. 5. The insets are necessary for impedance to match with the port. The insets dimension is 0.2 mm × 0.15 mm. Finally, a waveguide port is designed to connect with the fed line. The receiver antenna is the mirror copy of the transmitter antenna. Both are placed face to face at 15 mm apart. The breast fantom is placed between the transmitter and the receiver antenna as shown in Fig. 4. As the designed sensor is very small in size so it can be incorporated in the middle of the printed circuit board (PCB) or on the edges. Hoever, the designed model would be more useful in 5G and beyond communications by making it an array of the prototype unit cell. To do so, 10, 16, or 18 elements of the array can be placed on the edges or on side frames of PCB to integrate with other electronic circuitry.

For creating a more precise image by mmWave imaging method, scattered microwave pulses must be received from many locations and directions. Other studies have used a different approach. The method described in [22] involves collecting scattered pulses by rotating an antenna around a fantom. It takes more time to collect scattered pulses with this method, and it's likely that mechanical defects will cause the antenna to end up in an unexpected error when it rotates the fantom, leading to a false tumor location being detected. In this study, 9 antennas are arrayed around a hemispherical of 18 mm in radius to evaluate the data in mmWave imaging.

To accommodate different range of breast sizes, the radius of the hemisphere can be increased or decreased. If the tumor is within the range of the antennas, it will be detected. To accomplish this, the positions of the antennas within the array have been chosen to provide coverage over the maximum volume of fantom. Fig. 7(a) depicts the top view of the array antenna layout. The array's 9 antennas are spaced as follows: the cross-sectional lengths h_1 and h_2 between the two antennas are 14 mm and 18 mm, respectively which is shown in Fig. 7(a). The cross-sectional angle α is considered as 90° in precise. There are five antennas in a row, considering the bottom antenna which is number 7 in 0°, providing each antenna with a $\theta = 40°$ separating from its nearest neighbor antenna shown in Fig. 7(b). Figs. 7(c) and 7(d), are the sides and back views of the array setup, respectively.

V. SIMULATION RESULTS AND DISCUSSIONS

A. S-PARAMETRIC ANALYSIS

Due to the variation in electrical properties of healthy breast fantom and malignant which are permittivity and permeability, the reflection coefficient is also varied. Because the electromagnetic wave reacts differently for different permittivity and permeability. Permittivity and conductivity are the basis for the electromagnetic sensing properties of breast phantoms. Complex permittivity plays an important role in determining the polarization effects of an incoming electromagnetic wave (EM wave), which is expressed as [20],

$$\varepsilon'(\omega) = \varepsilon'_\infty + \left(\frac{\varepsilon'_s - \varepsilon'_\infty}{1 + \omega^2\tau^2}\right) \tag{5}$$

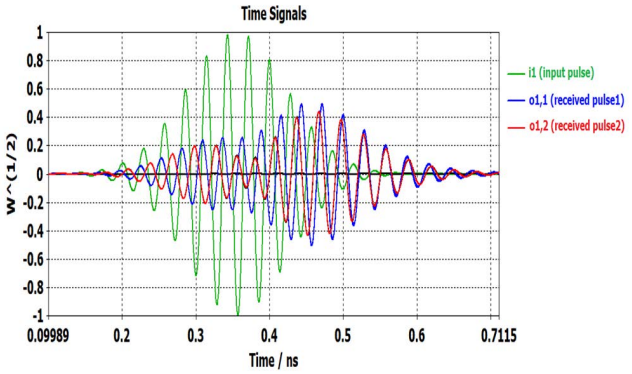

FIGURE 8. Normalized time domain transmitted and received pulse in face-to-face setup.

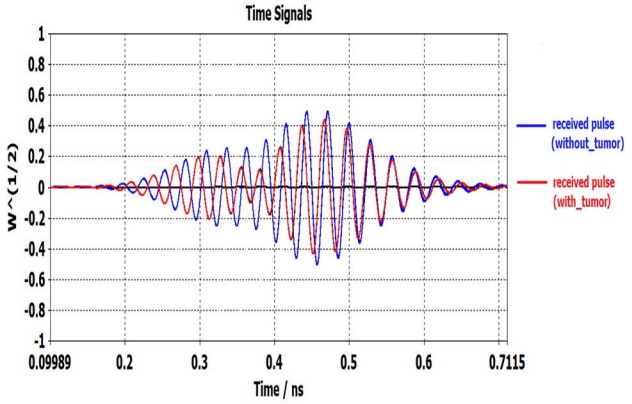

FIGURE 9. Variation in received pulse in the presence of tumor cell.

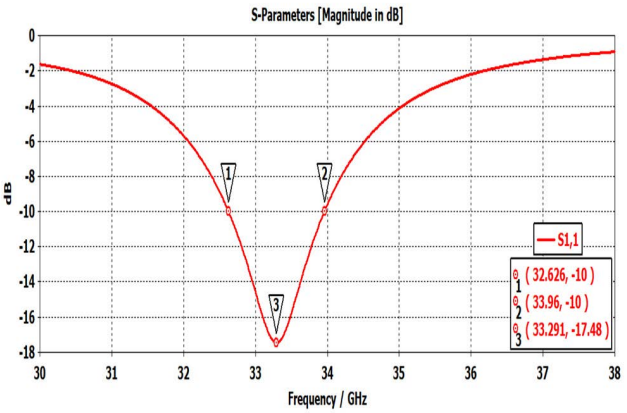

FIGURE 10. Parametric study of S-parameter ($S_{1,1}$) of the proposed antenna.

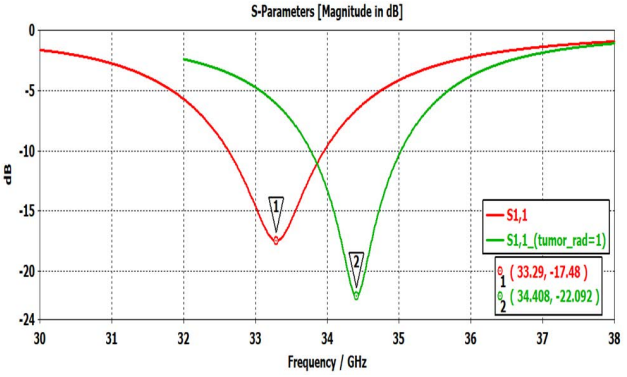

FIGURE 11. Variation of S-parametric resonant frequency for 1 mm of tumor placed inside breast fantom.

The breast tissue's relative permittivity and conductivity vary with the angular frequency (ω) of the incoming electromagnetic pulse. Specifically, the real and imaginary components of the relative permittivity are denoted by ε_s' and ε_∞', respectively. The electron's mean cross-medium relaxation time is denoted by τ.

The preceding formula shows how the antenna sensor's operating frequency and the phantom model's permittivity are crucial to cancer detection. When mmWave frequency contact with the phantoms, there is a substantial discrepancy in the relative permittivity of healthy and cancerous breast tissue and for that reason, the S-parameter value varies. Fig. 8 shows the normalized transmitted and received pulses by face-to-face transmitter and receiver antennas. The receiver antenna received a time-delayed and attenuated signal of input. However, when the tumor cell is presented inside the breast fantom, the received signal is distorted slightly as shown in Fig. 9. The proposed antenna's simulated ($|S_{11}|$ (dB)) result is shown in Fig. 10. The operating bandwidth of the antenna is 32.626 GHz to 33.96 GHz and the resonant frequency occurred at 33.291 GHz which covers the 5G Communication application and satellite application bands (26.5-40 GHz). If $S_{1,1}$ is below -10 dB, then at least 90% of the input power is delivered to the antenna. This suggests that the S-parametric values are obtained is acceptable. $S_{1,1}$ represents the amount of reflected power the device is intending to send to the antenna. In free space, the antenna simulation produces a resonant frequency at 33.29 GHz with a reflection coefficient of -17.48 dB and the value of Voltage Standing Wave Ratio (VSWR) is 1.31.

In the CST environment, the breast fantom is created and the receiving and transmitting antenna is placed on both sides of the breast fantom. A tumor in the shape of a sphere is placed inside the phantom. The tumor has dielectric permittivity and conductivity of 18 and 1.05 S/m. Fig. 10 shows the ideal resonant frequency of the antenna, which is sifted from 33.29 GHz to 34.408 GHz when a 1 mm tumor cell is detected in the breast fantom that is depicted in Fig. 11 as well. When the tumor size is increased inside the breast fantom, the ideal resonant frequency is varied significantly. Fig. 12 shows the result for 1 mm and 2 mm of tumor sizes placed inside the breast model. In Fig. 13 the close view is shown that when the tumor size is increased from 1 mm to 2 mm, the resonant frequency is shifted from 34.408 GHz to 34.464 GHz.

For 3 mm of tumor size, the resonant frequency is shifted to 34.536 GHz which is shown in Fig. 14. In Fig. 15 shows the close view image of shifted resonant frequency for 1 mm,

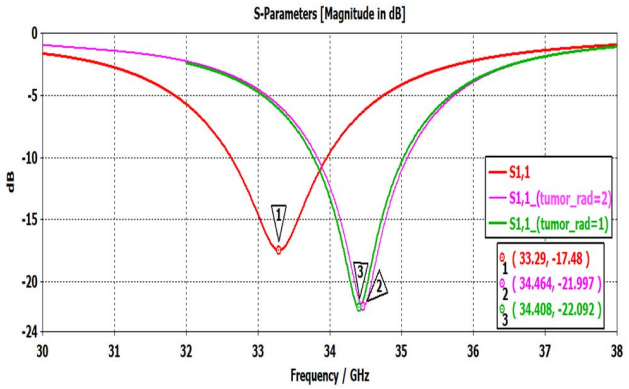

FIGURE 12. Variation of S-parametric resonant frequency for 1 to 2 mm of tumor cell placed inside the breast fantom.

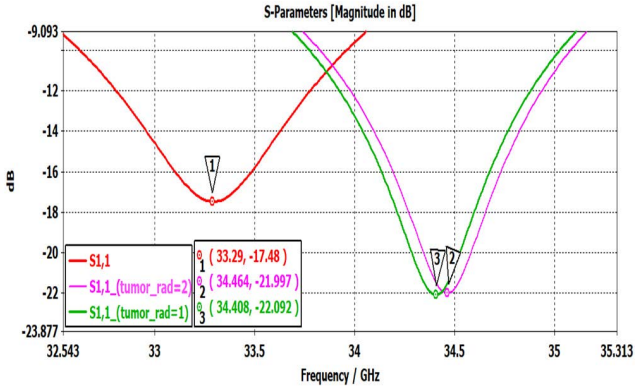

FIGURE 13. Close view of S-parametric shift for 1 to 2 mm of tumor placed inside breast fantom.

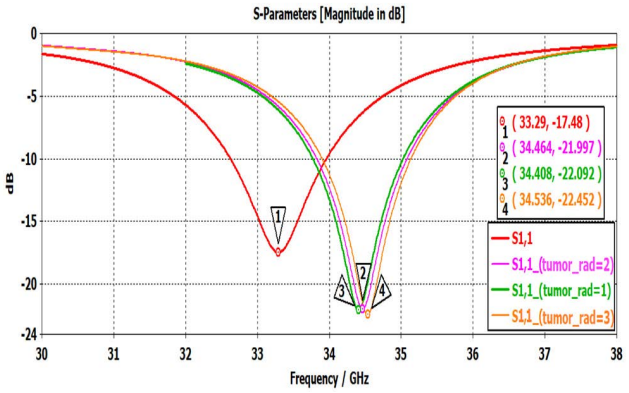

FIGURE 14. Variation of S-parametric resonant frequency for 1 to 3 mm of tumor cell placed inside the breast fantom.

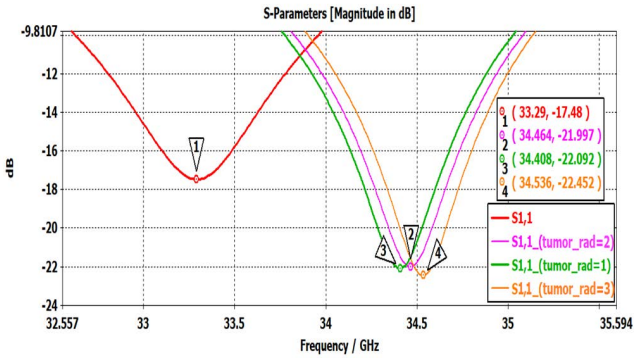

FIGURE 15. Close view of S-parametric shift for 1 to 3 mm of tumor cell placed inside breast fantom.

TABLE 2. Shifted resonant frequency with the tumor size.

Tumor Size (mm)	0	1	2	3
Resonant Frequency (GHz)	33.291	34.408	34.464	34.536
Reflection Coefficient (dB)	-17.48	-22.092	-21.997	-22.452

2 mm, and 3 mm of tumor size, respectively. If the tumor size increases more, then the resonant frequency of the antenna will be more distorted and varied. So, from the result analysis, it can be said that this designed antenna sensor is capable of detecting the presence of a very tiny malignant precisely which is 1 mm in size. So, it is possible to detect breast cancer or breast tumor at a very early stage and millions of lives can be saved worldwide. As a result, the proposed antenna can function as a bio-sensor in the field of biomedical imaging. In the simulation, the tumor size varied from 1 mm to 3 mm in radius. Table 2 shows the variation of the frequency with the change of tumor size inside the breast fantom.

Fig. 16 represents the S-parameters ($S_{1,1}$, $S_{2,1}$, $\cdots$ $S_{9,1}$) response when antenna one is excited and the other 8 antennas are receiving the scattered signals in the presence of tumor in breast fantom. Signal $S_{1,1}$ is the reflected signal of antenna-1. Signal $S_{2,1}$ is backscattered from antenna-1 and picked up by antenna-2, $S_{3,1}$ is backscattered from antenna-1 and picked up by antenna-3, $S_{9,1}$ is backscattered from antenna-1 and picked up by antenna-9, and so on. As the array model has 9 elements in total as shown in Fig. 7, the total number of S-parameters are $9^2 = 81$ and these are multiplied by 3 different tumor sizes which are 243 scattered signals in total. That massive number of signals cannot be represented in a single graph. There are significant shifts and changes in S-parameters of the transmitter antennas due to the presence of the tumor cell in breast fantom. Those distortions in S-parameters ($S_{1,1}$, $S_{2,2}$.... $S_{9,9}$) are presented in Fig. 17. Some of the S-parameters ($S_{4,4}$, $S_{6,6}$, $S_{7,7}$) are presented in Fig. 18 for a better view.

Because the tumors have higher dielectric characteristics than normal breast tissues, the scattered signals are distinct. Therefore, the suggested antenna and antenna array system design are promising options for breast imaging due to their capacity to detect tumors by thoroughly examining S-parameter signals. The imaging S-parameters signal data is then evaluated and processed with the IC-DAS image beamforming algorithm technique implemented in the MATLAB

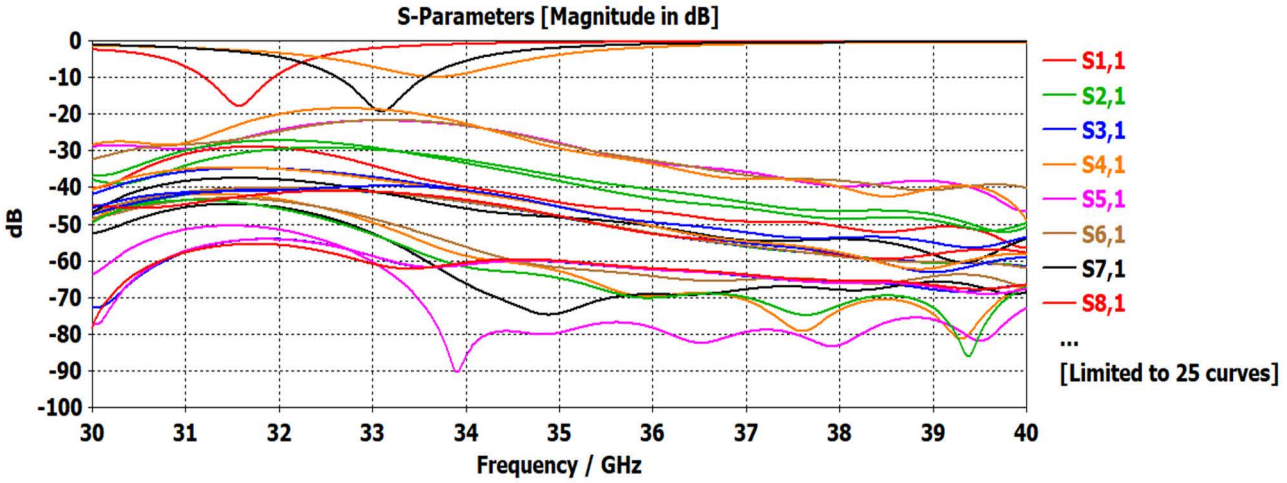

FIGURE 16. S-parameters of the array antenna setup.

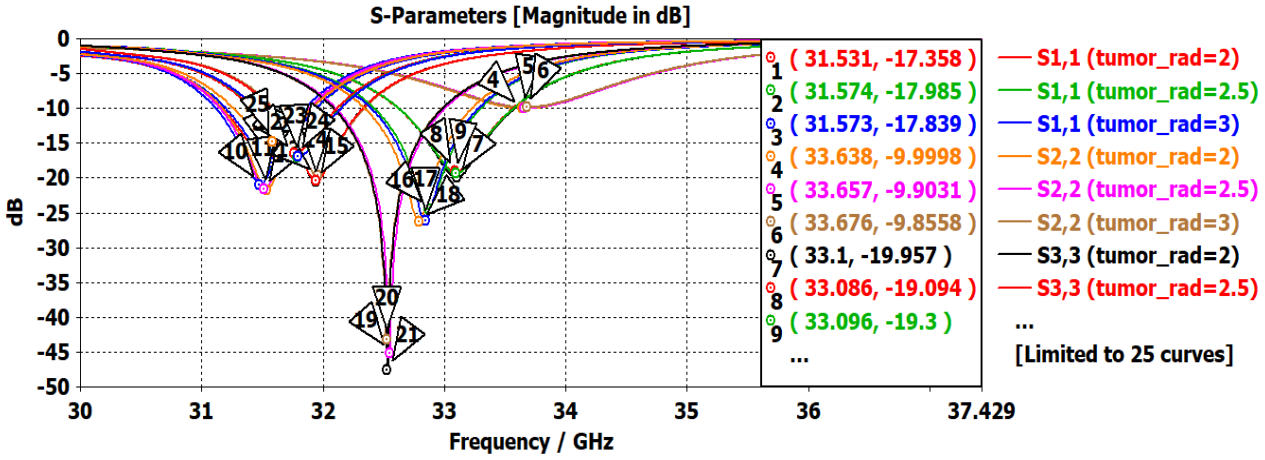

FIGURE 17. S-parameters of the 9 elements array-antenna setup with the presence of different tumor sizes (2mm, 2.5mm, 3mm).

environment [3]. Fig. 19 shows the imaging outcome of the targeted tumor, after the data has been processed by the algorithm for 2 mm of tumor cell. Fig. 19 shows the rebuilt photo of a breast phantom with a tumor size of 2 mm. It is verified that the intended tumor has been found and marked with a bright red hue. It is evident that our proposed technology can be a good contender for mmWave breast imaging to detect the tumor by carefully analyzing the S-parametric data.

B. SPECIFIC ABSORPTION RATE ANALYSIS

The Specific Absorption Rate (SAR) refers to the rate of absorption of non-ionizing RF power per unit mass in human body tissues expressed as (6). When a biological tissue mass is exposed to an electromagnetic field, it absorbs radiation energy is quantified by SAR [21].

$$SAR_{local}(\vec{r},\omega) = \frac{\sigma(\vec{r},\omega)\langle E(\vec{r},\omega)\rangle^2}{2\rho(\vec{r})} \tag{6}$$

where E represents electric field strength (V/m), $\sigma\ (\vec{r},\omega)$ represents the material's electrical conductivity (S/m), $\vec{r}$ is the position vector, $\rho(\vec{r})$ represents the tissue density at$\vec{r}$ (kg/m^3) and ω is the frequency. The unit of measurement for SAR is W/kg.

The SAR is averaged over a small sample volume either 1 gram(g) of the modelled biological tissues in Australia and the United States, or 10 gram(g) in Europe and Japan recommended by IEEE STDP1528.4. The spatial peak value of non-occupational exposure does not exceed 1.6 W/kg for 1g (Australia, USA) or 2.0 W/kg for 10g (Japan) [21]. The average SAR can be expressed as,

$$SAR_{average}(\vec{r},\omega) = \frac{1}{V}\int \frac{\sigma(\vec{r},\omega)\langle E(\vec{r},\omega)\rangle^2}{\rho(\vec{r})} d\vec{r} \tag{7}$$

where V refers to the volume in m^3.

SAR analysis is carried out by positioning the mmWave antenna adjacent to the breast phantoms and using a CST

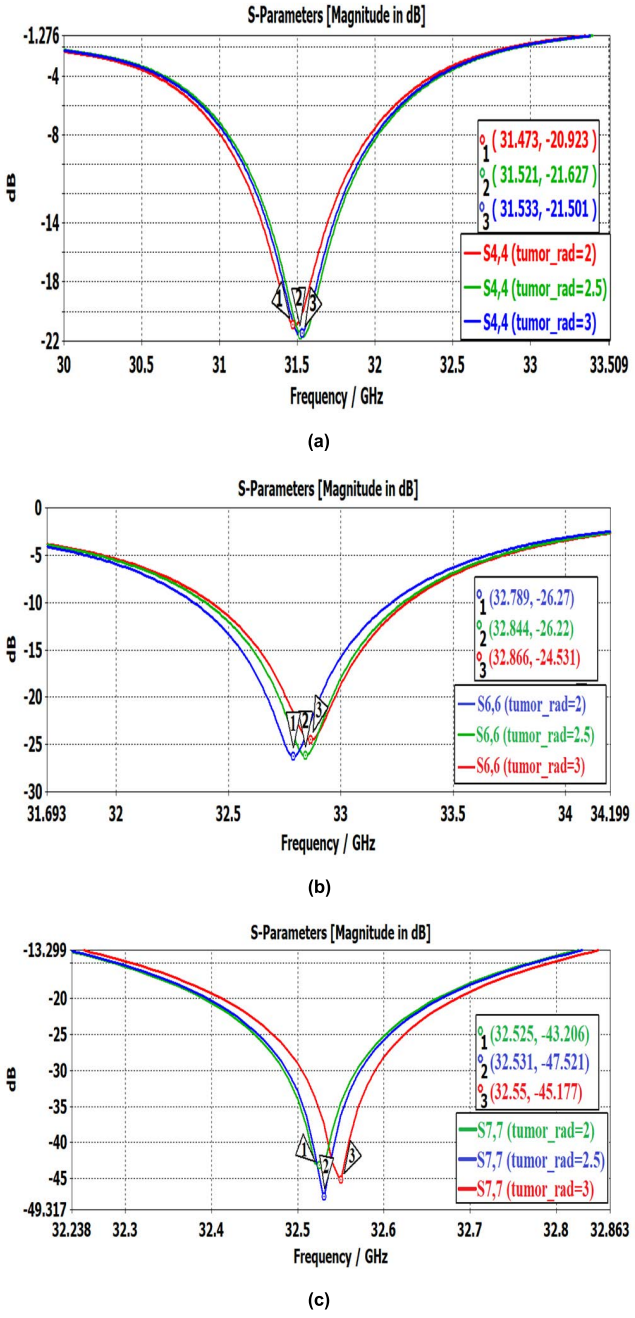

FIGURE 18. Some specific S-parametric shifts of the array-antenna ($S_{4,4}$, $S_{6,6}$, $S_{7,7}$).

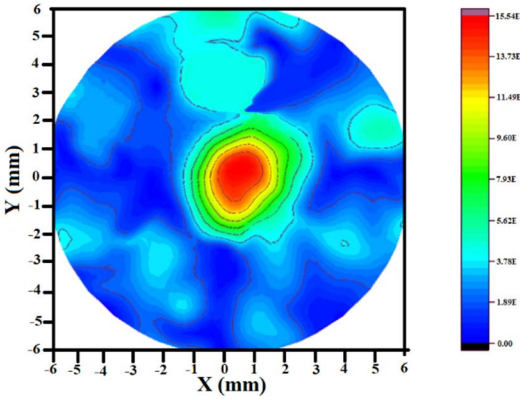

FIGURE 19. Reconstructed image of circular breast fantom using DAS beamforming algorithm.

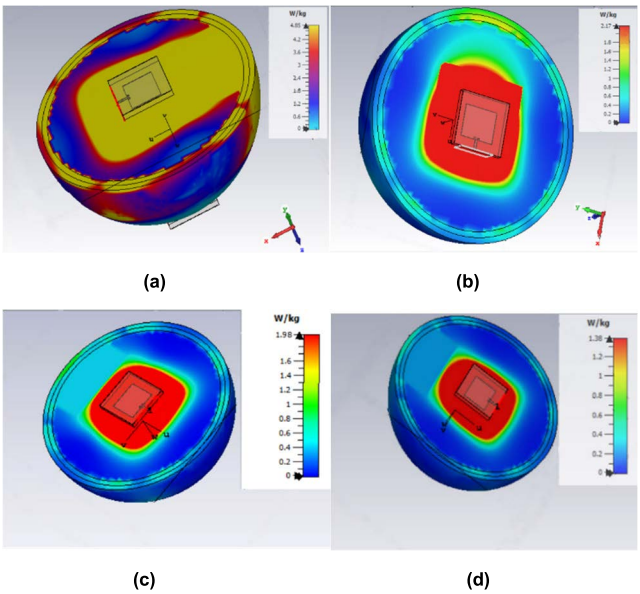

FIGURE 20. SAR analysis of the anatomical fantom in CST: (a) antenna sensor placed at a closer distance of the fantom, (b) antenna sensor placed at an optimized distance of the fantom, (c) SAR value for 1g of unit mass, and (d) SAR value for 10g of unit mass.

parametric sweep to adjust the distance and power levels between the antenna and the breast models. Best optimized microwave exposure results can be used in real-life patients as well as bio-medical applications. Figs. 20 and 21 show the SAR analysis of this system.

The simulation setup described here has been proposed for the use in biomedical studies. As a result, the SAR of the proposed system on breast tissues is examined. Fig. 20 illustrates the SAR results for the antenna radiating at the resonant frequency while a breast phantom is present. The SAR value is analyzed when the antenna radiates towards the phantom directly. Figs. 20(a) and 20(b) show that, at the resonant frequencies, the breast phantom's SAR exceeds 2 W/kg. By adjusting the distance between the antenna sensor and breast fantom the value is taken down to 1.98 W/kg for 10 g of body tissue and 1.38 W/kg for 1 g of body tissue as shown in Figs. 20(c) and 20(d), respectively. Consequently, the antenna is completely safe for human use (below 1.6 W/Kg for 1 g or below 2 W/kg for 10g) and well-suited to the intended biomedical applications.

Fig. 22 shows the cross-sectional view of SAR analysis of the breast fantom. In the color image, the SAR value of tumor cell and some healthy tissues seems to be the same exposure. Besides, in this research, the tumor cell is considered as a symmetrical circular shape. However, in the real life, the

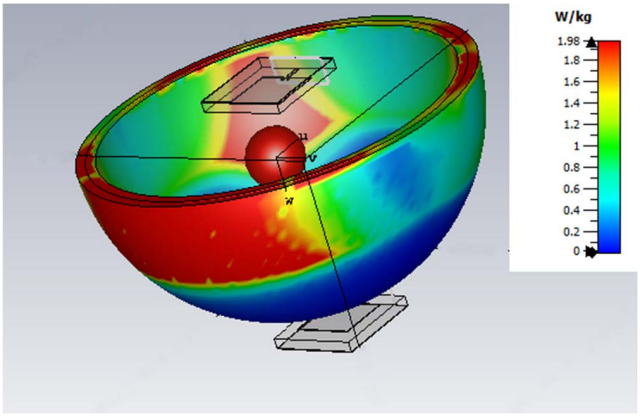

FIGURE 21. SAR imaging result of the breast fantom with tumor cell.

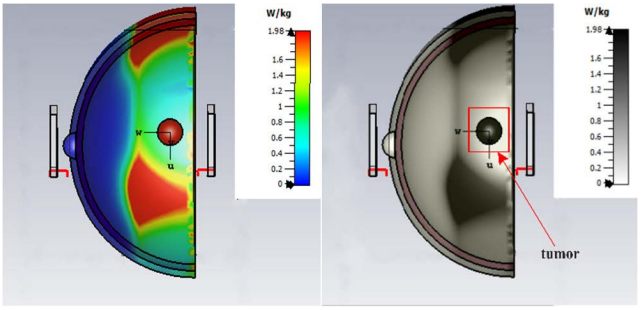

FIGURE 22. Precise malignant location detection in gray-scale imaging.

tumor cells are not always symmetrical but asymmetrical shapes in many cases. For that reason, the SAR value will be scattered more and the exact location of the tumor may be miscalculated. Therefore, in a grayscale image, the contrast of the tumor is different from healthy tissues for its different dielectric properties as shown in Fig 22(b). So, the tumor location is determined 100% accurately in the grayscale image.

Fig. 23 shows the omnidirectional far-field radiation pattern of the antenna at 30 GHz and 35 GHz, which is uniform and linearly polarized. That kind of radiation pattern also helps to locate the tumor cells precisely because of its scanning capability.

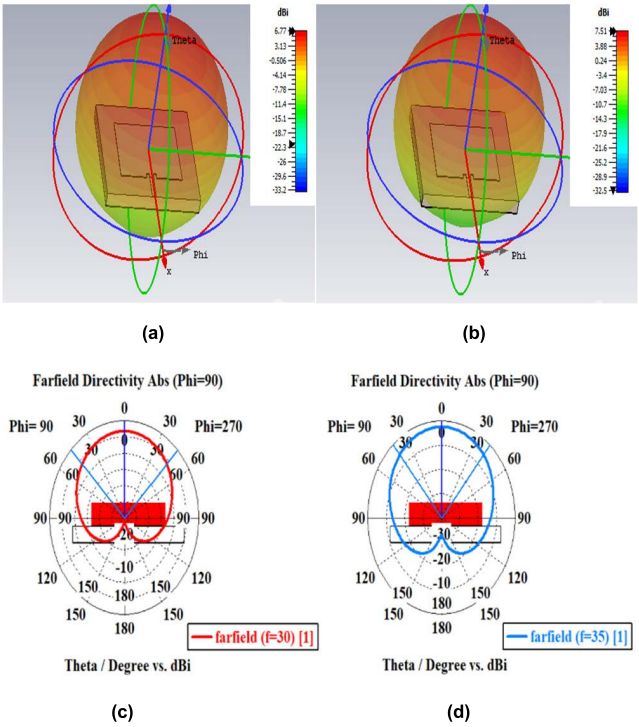

FIGURE 23. The radiation pattern of the proposed antenna, (a) 3-D radiation pattern at 30 GHz, (b) 3-D radiation pattern at 35 GHz, (c) 2-D radiation pattern at 33 GHz, and (d) 2-D radiation pattern at 35 GHz.

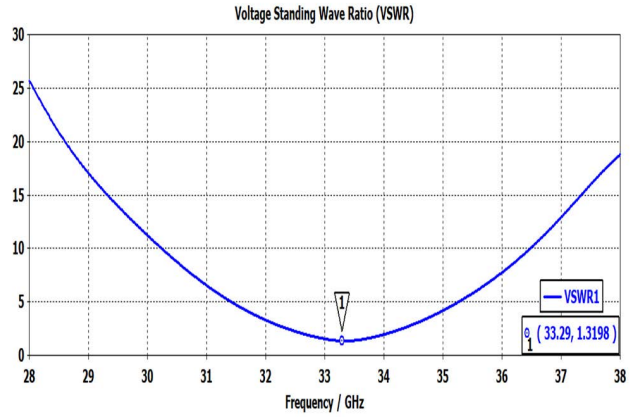

FIGURE 24. VSWR value of the proposed single element antenna at resonant frequency.

C. 5G COMPATIBILITY ANALYSIS

At the resonant frequency of 33.29 GHz, the VSWR is 1.31, making it an ideal device for stable 5G wireless communication and beyond. If the impedance of the antenna and its transmission line is mismatched, power will be dissipated inefficiently. When the VSWR is high, the impedance mismatch is also large. Fig. 24 displays the antenna's VSWR reading of 1.3 which indicates the antenna is well designed. From Fig. 25, it can be observed that the gain of the antenna is 6.64 dB and the directivity of the antenna is found 7.26 dBi as shown in Fig. 26 as well. So, the efficiency ($\frac{gain}{directivity}$) of this antenna sensor is 91.46% which is much better than many recent works.

A larger frequency range (>24GHz) is necessary for the exceptionally fast data transfer speeds of 5G and later communications [23]. The designed antenna sensor operates in the higher frequency band (>32 GHz) which is very high compared to some recent works [24], [25], [26]. At the resonant frequency of 33.29 GHz, the VSWR is 1.31, making it an ideal system for stable 5G and beyond wireless communication. Therefore, the antenna system is better suited to the requirements of 5G and beyond

TABLE 3. Comparison table with existing literature.

Refference	Dimension (mm^3)	Operating Frequency (GHz)	Gain (dB)	Efficiency (%)	Tumor detection Stage (T_1-T_4)	Imaging Method	Applications
[27]	30 × 25 × 1.6	2.70–10.30	5.50	80 %	> T_3	S-parametric analysis	Microwave breast imaging
[28]	24 × 22 × 1.6	3.04–11.43	5.10	> 82 %	----	S-parametric analysis	Microwave imaging
[29]	40 × 40 × 1.6	2.50–11.00	7.20	----	>T_2	Backscattered MERIT imaging algorithm	Microwave breast imaging
[30]	29 × 24 × 1.5	2.80–11.50	5.80	82%	----	S-parametric analysis	Microwave imaging
[31]	44 × 52.4× 1.6	3.5–15.0	----	----	T_2 (5 mm)	Confocal Imaging	Microwave breast imaging
[32]	40 × 40 × 1.6	3.01–11.0	7.06	92%	T_3 (10 mm)	DMAS algorithm	Microwave breast imaging
[3]	51 × 42 × 1.57	2.80–7.00	6.20	---	>T_2	IC-DAS	Microwave breast imaging
[33]	88 × 75 × 1.6	1.54–7.00	8.50	92%	T_3 (10 mm)	Backscattered signal imaging algorithm	Microwave breast imaging
[34]	27 × 29 × 1.6	3-15	---	---	T_2	SAR analysis	Microwave breast imaging
[18]	30 × 40 × 1.6	2.8-20	---	----	T_3 (10 mm)	S-parametric analysis and SAR analysis	mmWave breast imaging
This paper	5 × 5 × 0.578	30-40	6.65	92%	T_1 (1 mm)	S-parametric analysis, IC-DAS and SAR analysis	mmWave breast imaging and 5G communication

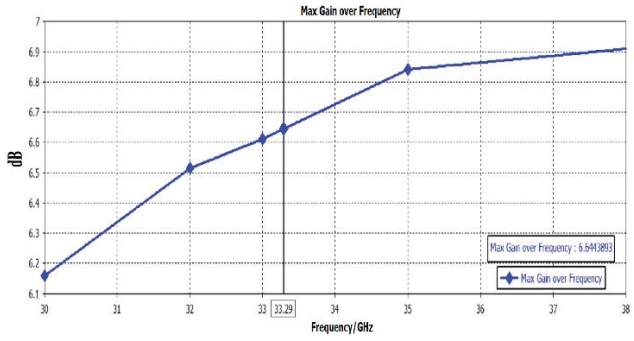

FIGURE 25. Simulated gain of the proposed single-element antenna.

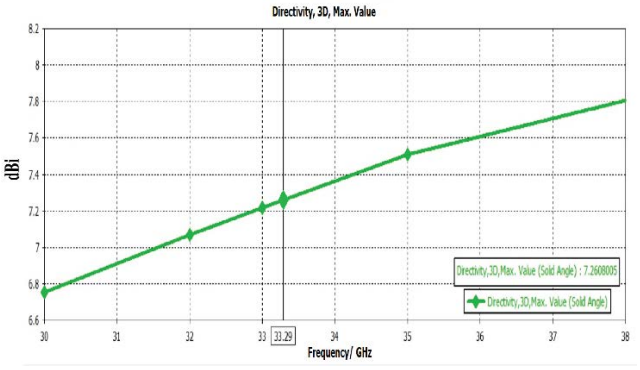

FIGURE 26. Simulated directivity value of the proposed single-element antenna.

communication technologies due to its higher frequency band operation and improved reflection coefficient. As the proposed design is very tiny, therefore, it can be incorporated with next-generation compact thin smartphones with multiple array elements for multiple-input multiple-output (MIMO) communication [25], [26]. The proposed antenna model has the significant potential to detect early-stage malignant in breast fantom.

It is also more convenient in 5G and beyond communication applications by making 10 or more elements of the array of the proposed prototype unit cell [26] because it is very small in size with better gain and efficiency compared to recent studies. It can be done by just duplicating the single-element antenna as the design is very convenient and simple. A comparative study with existing literatures is given in Table 3. Compared to the other works, the proposed antenna has the characteristics of a lower dimension in size, higher operating frequency, higher efficiency, and capability of smaller-size tumor detection. Moreover, the proposed scheme considers three type of imaging methods whereas other works consider two or one. As the size of the antenna is so miniaturized, it will require a very sophisticated fabrication process and a network analyzer that operates in high frequencies (>30 GHz) to measure the S-parameters and other required results. The performance of the antenna sensor can be increased by making more array elements as well.

VI. CONCLUSION

The spreading of breast cancer is alarming around the world, and it is mostly responsible for the lack of awareness and

easily accessible portable medical equipment that can help women detect any abnormal changes in their breasts at an early stage. In order to address the pressing demand for mmWave antennas, a very simple design, low-cost, and easy-to-use antenna sensor is designed. The antenna is fabricated on a dielectric substrate called ''Roger RT 5880'' in CST simulation software. The overall dimension of the antenna is 5×5 mm^2 and the antenna has a bandwidth of 1.34 GHz (32.626–33.96 GHz) along with a high gain and directivity. The sensor works at a frequency of 33.29 GHz and can detect the tumor cell inside the breast which is 1 mm in size. This sensor can detect a suspected tumor location deep into the breast by using uniform changes in the S-parameter data of the antennas. The antenna has a higher gain of 6.64 dBi and has stable radiation efficiency which means that the antenna has the ability to operate for 5G and beyond communication systems. Overall, the antenna is low profile, compact in size, higher operating bandwidth which is suitable for both microwave imaging and 5G applications.

REFERENCES

[1] F. Bray, J. Ferlay, I. Soerjomataram, R. L. Siegel, L. A. Torre, and A. Jemal, ''Global cancer statistics 2018: GLOBOCAN estimates of incidence and mortality worldwide for 36 cancers in 185 countries,'' *CA, Cancer J. Clin.*, vol. 68, no. 6, pp. 394–424, 2018.

[2] C. P. Wild, E. Weiderpass, and B. W. Stewart. *World Cancer Report: Cancer Research for Cancer Prevention*. Accessed: Mar. 25, 2022. [Online]. Available: https://publications.iarc.fr/Non-Series-Publications/WorldCancer-Reports/World-Cancer-Report-Cancer-Research-For-Cancer-Prevention-2020

[3] M. T. Islam, M. Z. Mahmud, M. T. Islam, S. Kibria, and M. Samsuzzaman, ''A low cost and portable microwave imaging system for breast tumor detection using UWB directional antenna array,'' *Sci. Rep.*, vol. 9, no. 1, p. 15491, Oct. 2019.

[4] M. E. Ladd, P. Bachert, M. Meyerspeer, and E. Moser, ''Pros and cons of ultra-high-field MRI/MRS for human application,'' *Prog. Nucl. Magn. Reson. Spectrosc.*, vol. 109, pp. 1–50, Dec. 2018.

[5] J. A. C. Desreux, ''Breast cancer screening in young women,'' *Eur. J. Obstetrics Gynecol. Reproductive Biol.*, vol. 230, pp. 208–211, Nov. 2018.

[6] R. L. Siegel, K. D. Miller, and A. Jemal, ''Cancer statistics, 2016,'' *CA Cancer J. Clin.*, vol. 66, no. 1, pp. 7–30, 2016.

[7] L. Wang, ''Microwave sensors for breast cancer detection,'' *Sensors*, vol. 18, no. 2, p. 655, Feb. 2018.

[8] E. C. Fear, J. Bourqui, C. Curtis, D. Mew, B. Docktor, and C. Romano, ''Microwave breast imaging with a monostatic radar-based system: A study of application to patients,'' *IEEE Trans. Microw. Theory Techn.*, vol. 61, no. 5, pp. 2119–2128, May 2013.

[9] A. Mirbeik-Sabzevari and N. Tavassolian, ''Tumor detection using millimeter-wave technology: Differentiating between benign lesions and cancer tissues,'' *IEEE Microw. Mag.*, vol. 20, no. 8, pp. 30–43, Aug. 2019.

[10] A. Mirbeik-Sabzevari, R. Ashinoff, and N. Tavassolian, ''Ultra-wideband millimeter-wave dielectric characteristics of freshly excised normal and malignant human skin tissues,'' *IEEE Trans. Biomed. Eng.*, vol. 65, no. 6, pp. 1320–1329, Jun. 2018.

[11] M. T. Bevacqua, S. Di Meo, L. Crocco, T. Isernia, and M. Pasian, ''Millimeter-waves breast cancer imaging via inverse scattering techniques,'' *IEEE J. Electromagn., RF Microw. Med. Biol.*, vol. 5, no. 3, pp. 246–253, Sep. 2021.

[12] M. Z. Chowdhury, M. K. Hasan, M. Shahjalal, M. T. Hossan, and Y. M. Jang, ''Optical wireless hybrid networks: Trends, opportunities, challenges, and research directions,'' *IEEE Commun. Surveys Tuts.*, vol. 22, no. 2, pp. 930–966, 2nd Quart., 2020.

[13] R. Przesmycki, M. Bugaj, and L. Nowosielski, ''Broadband microstrip antenna for 5G wireless systems operating at 28 GHz,'' *Electronics*, vol. 10, no. 1, p. 1, Dec. 2020.

[14] A. F. Kaeib, N. M. Shebani, and A. R. Zarek, ''Design and analysis of a slotted microstrip antenna for 5G communication networks at 28 GHz,'' in *Proc. 19th Int. Conf. Sci. Techn. Autom. Control Comput. Eng. (STA)*, Mar. 2019, pp. 648–653.

[15] N. Sobhani, C. Fan, P. O. Flores-Villanueva, D. Generali, and Y. Li, ''The fibroblast growth factor receptors in breast cancer: From oncogenesis to better treatments,'' *Int. J. Mol. Sci.*, vol. 21, no. 6, p. 2011, Mar. 2020.

[16] Y. Feng, M. Spezia, S. Huang, C. Yuan, Z. Zeng, L. Zhang, X. Ji, W. Liu, B. Huang, W. Luo, B. Liu, Y. Lei, S. Du, A. Vuppalapati, H. H. Luu, R. C. Haydon, T.-C. He, and G. Ren, ''Breast cancer development and progression: Risk factors, cancer stem cells, signaling pathways, genomics, and molecular pathogenesis,'' *Genes Diseases*, vol. 5, no. 2, pp. 77–106, Jun. 2018.

[17] *How Fast Does Breast Cancer Grow and Spread?* Verywell Health. Accessed: May 17, 2022. [Online]. Available: https://www.verywellhealth.com/breast-cancer-growth-rate-4175666

[18] T. Kuroishi, S. Tominaga, T. Morimoto, H. Tashiro, S. Itoh, H. Watanabe, M. Fukuda, J. Ota, T. Horino, T. Ishida, T. Yokoe, K. Enomoto, Y. Kashiki, and M. Ogita, ''Tumor growth rate and prognosis of breast cancer mainly detected by mass screening,'' *Jpn. J. Cancer Res.*, vol. 81, no. 5, pp. 454–462, May 1990.

[19] V. Selvaraj, P. Srinivasan, J. Kumar, R. Krishnan, and K. Annamalai, ''Highly directional microstrip ultra wide band antenna for microwave imaging system,'' *Acta Graphica*, vol. 28, no. 1, pp. 35–40, Jul. 2017.

[20] M. K. Sharma, M. Kumar, J. P. Saini, D. Gangwar, B. K. Kanaujia, and S. P. Singh, ''Experimental investigation of the breast phantom for tumor detection using ultra-wide band–MIMO antenna sensor (UMAS) probe,'' *IEEE Sensors J.*, vol. 20, no. 12, pp. 6745–6752, Jun. 2020.

[21] V. Kumari, G. Sheoran, and T. Kanumuri, ''SAR analysis of directive antenna on anatomically real breast phantoms for microwave holography,'' *Microw. Opt. Technol. Lett.*, vol. 62, no. 1, pp. 466–473, Jan. 2020.

[22] J. Bourqui, J. M. Sill, and E. C. Fear, ''A prototype system for measuring microwave frequency reflections from the breast,'' *Int. J. Biomed. Imag.*, vol. 2012, Apr. 2012, Art. no. 851234.

[23] Z. Mohammad, N. Sarker, and C. Das, ''Design and analysis of a double slotted with multiple strips vivaldi antenna for high-speed 5G communications,'' in *Proc. IEEE Int. Conf. Telecommun. Photon. (ICTP)*, Dec. 2019, pp. 1–4.

[24] V. Thakur, N. Jaglan, and S. D. Gupta, ''Side edge printed eight-element compact MIMO antenna array for 5G smartphone applications,'' *J. Electromagn. Waves Appl.*, vol. 36, no. 12, pp. 1685–1701, Aug. 2022.

[25] N. Jaglan, S. D. Gupta, B. K. Kanaujia, and M. S. Sharawi, ''10 element sub-6-GHz multi-band double-T based MIMO antenna system for 5G smartphones,'' *IEEE Access*, vol. 9, pp. 118662–118672, 2021.

[26] N. Jaglan, S. D. Gupta, and M. S. Sharawi, ''18 element massive MIMO/diversity 5G smartphones antenna design for sub-6 GHz LTE bands 42/43 applications,'' *IEEE Open J. Antennas Propag.*, vol. 2, pp. 533–545, 2021.

[27] M. Z. Mahmud, M. T. Islam, A. F. Almutairi, M. Samsuzzaman, U. K. Acharjee, and M. T. Islam, ''A parasitic resonator-based diamond-shaped microstrip antenna for microwave imaging applications,'' *Electronics*, vol. 8, no. 4, p. 434, Apr. 2019.

[28] M. Ojaroudi and O. A. Civi, ''Bandwidth enhancement of small square monopole antenna using self-complementary structure for microwave imaging system applications,'' *Appl. Comput. Electromagn. Soc. J. (ACES)*, vol. 30, no. 12, pp. 1360–1365, Dec. 2015.

[29] M. Samsuzzaman, M. T. Islam, M. T. Islam, A. A. S. Shovon, R. I. Faruque, and N. Misran, ''A 16-modified antipodal Vivaldi antenna array for microwave-based breast tumor imaging applications,'' *Microw. Opt. Technol. Lett.*, vol. 61, no. 9, pp. 2110–2118, 2019.

[30] A. Hossain, M. T. Islam, A. F. Almutairi, M. S. J. Singh, K. Mat, and M. Samsuzzaman, ''An octagonal ring-shaped parasitic resonator based compact ultrawideband antenna for microwave imaging applications,'' *Sensors*, vol. 20, no. 5, p. 1354, Mar. 2020.

[31] T. Sugitani, S. Kubota, A. Toya, X. Xiao, and T. Kikkawa, ''A compact 4×4 planar UWB antenna array for 3-D breast cancer detection,'' *IEEE Antennas Wireless Propag. Lett.*, vol. 12, pp. 733–736, 2013.

[32] M. T. Islam, M. Samsuzzaman, M. T. Islam, S. Kibria, and M. J. Singh, ''A homogeneous breast phantom measurement system with an improved modified microwave imaging antenna sensor,'' *Sensors*, vol. 18, no. 9, p. 2962, Sep. 2018.

[33] M. T. Islam, M. Z. Mahmud, N. Misran, J.-I. Takada, and M. Cho, "Microwave breast phantom measurement system with compact side slotted directional antenna," *IEEE Access*, vol. 5, pp. 5321–5330, 2017.
[34] S. Subramanian, B. Sundarambal, and D. Nirmal, "Investigation on simulation-based specific absorption rate in ultra-wideband antenna for breast cancer detection," *IEEE Sensors J.*, vol. 18, no. 24, pp. 10002–10009, Dec. 2018.

CHINMOY DAS received the B.Sc. degree in electrical and electronic engineering from the Bangladesh University of Business & Technology (BUBT), Dhaka, Bangladesh, in April 2019. He is currently pursuing the M.Sc. degree in electrical and electronic engineering with the Khulna University of Engineering & Technology (KUET), Khulna, Bangladesh. He was a Former Runner-Up in the Mathematics Olympiad Contest-2014 at the National Level. He has successful done several projects, such as remote-control aircraft design, android device-controlled robot, noise cancellation sensor, gas leakage detection system, color object detection robot, water level detection system, RFID-based security system, password-based door lock system, fire alarm system, android-based home automation, smart car parking system, and density-based modern traffic control system. He has published 15 peer-reviewed research papers in international conferences and journals. He served as a Faculty Member at BUBT for almost one year, in 2021. His research interests include wireless communications and networking, wireless sensor networks, mmWave and terahertz antenna, and 5G and beyond antenna technology. He also received the Academic Excellence Award for his Excellent Academic Performance.

MOSTAFA ZAMAN CHOWDHURY (Senior Member, IEEE) received the B.Sc. degree in electrical and electronic engineering from the Khulna University of Engineering & Technology (KUET), Bangladesh, in 2002, and the M.Sc. and Ph.D. degrees in electronics engineering from Kookmin University, South Korea, in 2008 and 2012, respectively. In 2003, he joined the Electrical and Electronic Engineering Department, KUET, as a Lecturer, where he is currently working as a Professor. He has been working as the Head of the Department of Biomedical Engineering, KUET, since April 2022. He was a Postdoctoral Researcher with Kookmin University, from 2017 to 2019, supported by the National Research Foundation, South Korea. He has published research articles in top quality journals, such as IEEE Communications Surveys and Tutorials, IEEE Transactions on Services Computing, IEEE Transactions on Intelligent Transportation Systems, IEEE Transactions on Instrumentation and Measurement, IEEE Systems Journal, *IEEE Communications Magazine*, IEEE Communications Letters, *IEEE Consumer Electronics Magazine*, IEEE Access, and *Scientific Reports* (nature). His research interests include convergence networks, QoS provisioning, small-cell networks, the Internet of Things, eHealth, 5G and beyond communications, and optical wireless communication. In 2008, he received the Excellent Student Award from Kookmin University. His three papers received the Best Paper Award at several international conferences around the world. He was involved in many Korean government projects. He received the Best Reviewer Award 2018 by *ICT Express* journal. Moreover, he received the Education and Research Award 2018 given by Bangladesh Community, in South Korea. He was the TPC Chair of the International Workshop on 5G/6G Mobile Communications, in 2017 and 2018. He has been serving as the Publicity Chair of the International Conference on Artificial Intelligence in Information and Communication, from 2019 to 2023, and International Conference on Ubiquitous and Future Networks, in 2022. He served as a reviewer for many international journals, including IEEE, Elsevier, Springer, ScienceDirect, MDPI, and Hindawi published journals and IEEE conferences. He has been working as an Editor for *ICT Express*, an Associate Editor of IEEE Access, an Associate Editor of *Frontiers in Communications and Networks*, a Lead Guest Editor for *Wireless Communications and Mobile Computing*, and a Guest Editor for *Applied Sciences*. He has served as a TPC member for many IEEE conferences.

YEONG MIN JANG (Member, IEEE) received the B.E. and M.E. degrees in electronics engineering from Kyungpook National University, South Korea, in 1985 and 1987, respectively, and the Ph.D. degree in computer science from the University of Massachusetts, USA, in 1999. He was with the Electronics and Telecommunications Research Institute, from 1987 to 2000. Since 2002, he has been with the School of Electrical Engineering, Kookmin University, Seoul, South Korea, where he has been the Director of the Ubiquitous IT Convergence Center, in 2005 and 2010, has been the Director of the LED Convergence Research Center, since 2010, has been the Director of the Internet of Energy Research Center, since 2018, and has been the Director of the AI Mobility Research Institute, since 2021. His research interests include 5G/6G mobile communications, internet of energy, the IoT platform, AI platform, eHealth, smart factory, optical wireless communications, optical camera communication, AI mobility, and the Internet of Things. He has organized several conferences and workshops, such as the International Conference on Ubiquitous and Future Networks, from 2009 to 2017, the International Conference on ICT Convergence, from 2010 to 2016, the International Conference on Artificial Intelligence in Information and Communication, since 2019, the International Conference on Information Networking, in 2015, and the International Workshop on Optical Wireless LED Communication Networks, from 2013 to 2016. He was a recipient of the Young Scientist Award from the Korean Government, from 2003 to 2006, and KICS Dr. Irwin Jacobs Award, in 2018. He had served as the Founding Chair of the Korean Institute of Communications and Information Sciences (KICS) Technical Committee on Communication Networks, in 2007 and 2008. He had served as the Executive Director of KICS, from 2006 to 2014, the Vice President of KICS, from 2014 to 2016, and the Executive Vice President of KICS, in 2018. He was the President of KICS, in 2019. He had been the Steering Chair of the Multi-Screen Service Forum, from 2011 to 2019, the Society Safety System Forum, from 2015 to 2021, and has been the ESG Convergence Forum, since 2022. He served as the Chairman of the IEEE 802.15 Optical Camera Communications Study Group, in 2014, and the IEEE 802.15.7m Optical Wireless Communications TG. So, he successfully published IEEE 802.15.7-2018 and ISO 22738:2020 standard. He is the Chairman of IEEE 802.15.7a Higher Rate and Longer Range OCC TG since 2020. He is the Editor-in-Chief of *ICT Express* (indexed by SCIE). He is a fellow of KICS.